

# Greenspan acoustic viscometer for gases

K. A. Gillis, J. B. Mehl,<sup>a)</sup> and M. R. Moldover<sup>b)</sup>

*Thermophysics Division, National Institute of Standards and Technology, Gaithersburg, Maryland 20899*

(Received 17 July 1995; accepted for publication 14 February 1996)

Double Helmholtz acoustic resonators, first proposed by Greenspan for measuring the viscosity of gases, were tested with helium, argon, and propane. Two different resonators were tested extensively with all three gases. For each of these instruments, the results for the viscosities of the three gases were consistent within  $\pm 0.5\%$  at pressures spanning the range 25–1000 kPa. Without calibration, the viscosities deduced from one viscometer were systematically 1% larger than data from the literature; the viscosities from the second viscometer were systematically 3% larger than data from the literature. If the systematic differences were removed for each viscometer by calibration with a single gas at a single temperature and pressure, then nearly all the results for both instruments would have fallen within  $\pm 0.5\%$  of the data from the literature. In these viscometers, the test gases are in contact with robust metal parts only; thus, these instruments are applicable to a very wide variety of gases over a very wide range of temperatures. [S0034-6748(96)03605-3]

## I. INTRODUCTION

Double Helmholtz acoustic resonators can be designed to have large viscous losses in the duct connecting the two chambers (see Fig. 1). When this is done, the frequency response of these resonators becomes a sensitive function of the viscosity of the gas within the resonator. We call such resonators “Greenspan viscometers” in honor of Greenspan’s conception of this method of measuring the viscosity of a gas.<sup>1</sup>

In 1953, Greenspan and Wimenitz<sup>1</sup> tested double Helmholtz acoustic resonators as viscometers. Their results for the kinematic viscosity of air differed from the literature values by as much as 38%, and they concluded that “the method described does not at present offer a satisfactory basis for an instrument for the measurement of viscosity.” In this work, we revisit the method using improved instrumentation, modeling, and control of the properties of the test gases. We now conclude that with calibration, the method is capable of yielding state-of-the-art results under a wide range of conditions. We suggest that further study of the method is warranted for developing a primary standard Greenspan viscometer. Such a standard would be a robust instrument that could be used to check the oscillating disk viscometer that is now used as a standard.

Our optimism is based on measurements of the frequency responses of four Greenspan viscometers, each tested with three gases (helium, argon, and propane) at pressures spanning the range 25–1000 kPa. Although all of the data were taken at ambient temperature (22 °C), they span a factor of 350 in viscous diffusivity. This range  $7 \times 10^{-7} \text{ m}^2 \text{ s}^{-1} < D_v < 2 \times 10^{-4} \text{ m}^2 \text{ s}^{-1}$  is displayed graphically in Fig. 2. (Here,  $D_v \equiv \eta/\rho$ , where  $\eta$  is the viscosity and  $\rho$  is the mass density.)

Of the four Greenspan viscometers, two were studied more extensively than the others. One, designated “viscom-

eter 1,” was the “best.” The other, designated “viscometer 0,” was the “worst.” The dimensions of these viscometers were accurately determined with a coordinate measuring machine. Thus, the viscosity could be deduced from these two viscometers without calibration. For each of these viscometers, the viscosities of all three gases were consistent within  $\pm 0.5\%$  except at the very lowest pressures. Without calibration, the viscosities from viscometer 1 were systematically 1% larger than data from the literature; the viscosities from viscometer 0 were systematically 3% larger than data from the literature. If the systematic differences were removed by calibration of each viscometer with a single gas at a single temperature and a single pressure above 100 kPa, then nearly all the results for both instruments would have fallen within  $\pm 0.5\%$  of the data from the literature.

To put the performance of these Greenspan viscometers in perspective, we note that an uncertainty of  $\pm 1\%$  is near the state of the art in gas viscometry. In a recent publication based on *ab initio* calculations for helium, Aziz and co-workers<sup>2</sup> argued that the viscosity of helium as determined by the best measurement to date was systematically in error by 0.3%. The inconsistencies among gas viscometers from various laboratories are usually much larger than 0.3%.

In the Greenspan viscometer, an acoustic transducer coupled to the chamber  $V_1$  forces the test gas to oscillate through a duct leading to a second chamber  $V_2$ . The oscillations are driven at frequencies near the Helmholtz resonance, which, in the lowest approximation, is

$$\omega_0^2 = \frac{c_0^2 A_d}{L_d} \left( \frac{1}{V_1} + \frac{1}{V_2} \right). \quad (1)$$

Here,  $c_0$  is the speed of sound in the gas,  $A_d$  is the cross sectional area of the duct, and  $L_d$  is the length of the duct. In the instruments described here,  $f_0 = \omega_0/(2\pi)$  falls in the range  $100 \text{ Hz} \leq f_0 \leq 200 \text{ Hz}$  when  $c_0 \approx 300 \text{ m/s}$ . This frequency range is a factor of 10 to 100 below the frequencies of other resonances that might complicate the analysis of the frequency response data; other resonances include acoustic

<sup>a)</sup>Also at Physics Department, University of Delaware, Newark, DE 19716.

<sup>b)</sup>Author to whom correspondence should be addressed.

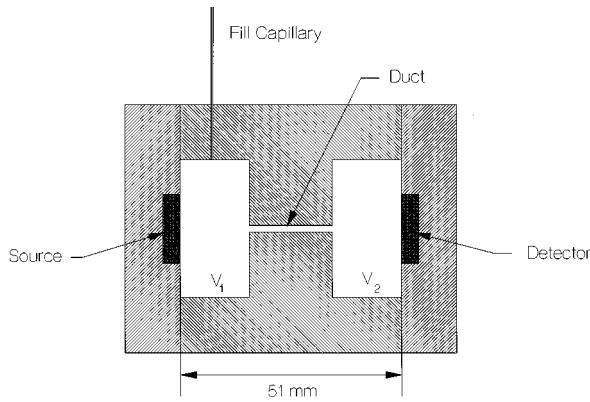


FIG. 1. Cross section of Greenspan viscometer 1.

resonances of the gas in the chambers, mechanical resonances in the transducers, and resonances in the mechanical structure of the Greenspan viscometer itself.

Most of the viscous dissipation occurs within the duct where the velocity of the gas is highest. Thus, the duct in the oscillating flow of the Greenspan viscometer plays a role analogous to that of the capillary tube in the unidirectional flow of the familiar Ubbelohde or Cannon–Fenske viscometers.<sup>3</sup> In particular, the duct's dimensions must be well known; the duct must be kept clean, and the effects of converging and diverging flows near the ends of the duct must be accounted for in the analysis of the data.

The viscosity is deduced from measurements of the frequency dependence of the acoustic pressure detected by an acoustic transducer coupled to the chamber  $V_2$  as the frequency of the acoustic source in  $V_1$  is scanned through the Helmholtz resonance (see Fig. 3). Thus, the frequency responses of the electroacoustic transducers must be known in

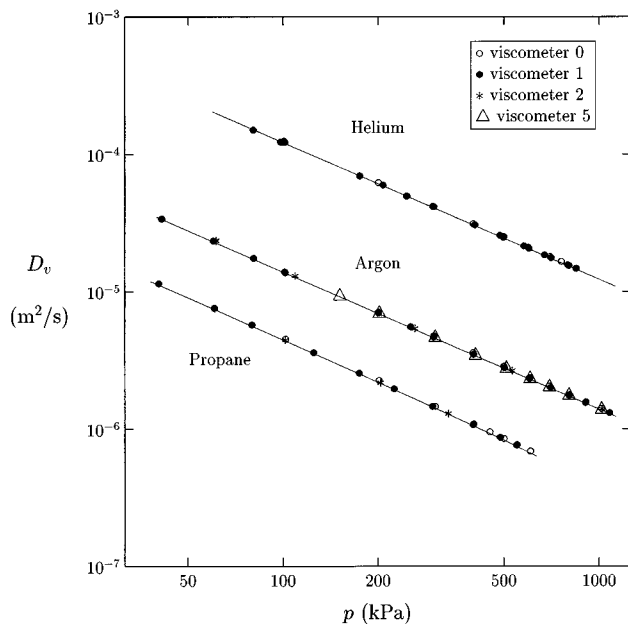


FIG. 2. The viscous diffusivity  $D_v \equiv \eta/\rho$  as a function of pressure for the gases studied. In some cases, data from several viscometers are superimposed.

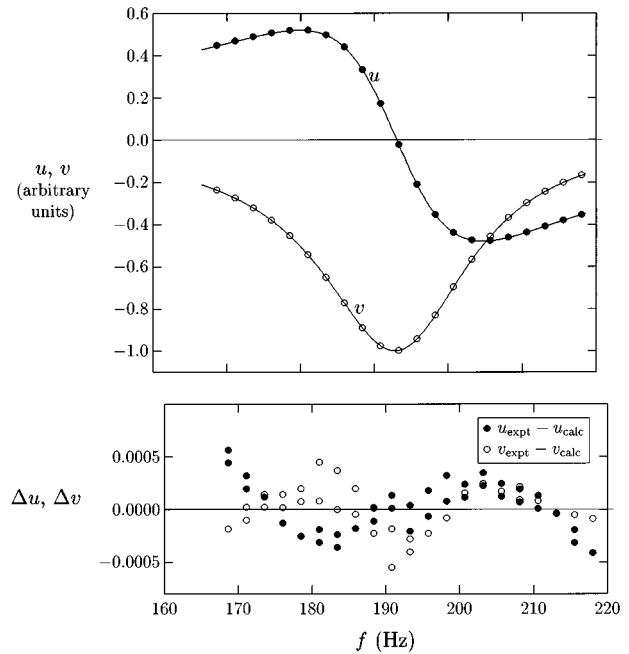


FIG. 3. Top: the real ( $u$ ) and imaginary ( $v$ ) components of  $V_{\text{detector}}/V_{\text{source}}$  as a function of the excitation frequency. These representative data were taken with argon in viscometer 1 at 295.9 K and 300.3 kPa. Bottom: deviations of  $u$  and  $v$  from a fit of Eq. (18) to the data shown above. The fractional deviations from the fit are all less than 0.0005.

the frequency range of interest. However, the transducers need not be calibrated. Indeed, they need not be stable for intervals longer than the minute or so required to measure the viscosity at a given temperature and pressure. In contrast, the differential pressure transducers used to determine the viscosity in unidirectional flow viscometers must be stable and calibrated.

To date, our experience indicates that the Greenspan viscometer operates well with  $Q$ 's of 10 or larger. [When the losses are not too large, the amplitude versus frequency response function is approximately Lorentzian. The  $Q$  is defined as  $f_0/(2g)$ , where  $2g$  is the full resonance width at  $1/\sqrt{2}$  of the maximum amplitude.] Thus, the transducers need to be characterized over a comparatively narrow frequency range. This easy-to-meet requirement together with the small values of  $f_0$  will facilitate the operation of future Greenspan viscometers with remote acoustic transducers coupled to the test gas via acoustic wave guides and diaphragms such as those described by Gillis and co-workers.<sup>4</sup>

Below, we provide a heuristic model useful for designing and understanding the operation of the viscometer. We report the results of a more detailed model that will be described elsewhere. We shall describe the test viscometers, the measurement procedures, and the test results. We conclude by discussing the potential for developing the Greenspan viscometer into a primary standard viscometer for gases.

## II. HEURISTIC MODEL

Here, we present a simple model for the Greenspan viscometer that is useful for insight and design purposes, but not for the most accurate analysis of data. When this model

is applicable, the resonance frequency of the double Helmholtz resonator is simply related to the speed of sound in the test gas and the half-width of the resonance is simply related to the viscosity of the test gas. The model is approximately correct for the experimentally important conditions in which both the viscous penetration length  $\delta_v$  and the thermal penetration length  $\delta_t$  are much smaller than the radius of the duct  $r_d$ . The penetration lengths are given by the relations:

$$\delta_v \equiv \sqrt{2\eta/\rho\omega} \quad (2)$$

and

$$\delta_t \equiv \sqrt{2\lambda/\rho C_p \omega}. \quad (3)$$

Here,  $\lambda$  is the thermal conductivity of the gas and  $\rho C_p$  is the constant-pressure heat capacity per unit volume of the gas.

We note that thermal effects within the duct are small because the acoustic temperature has a node in the duct that corresponds to the velocity antinode there. In some geometries, the thermal losses may be important; the detailed acoustic model shows this quantitatively.

In the lowest order approximation, one may consider the gas in the duct to be the inertial element of an oscillator and the pressure difference between the two chambers to provide the stiffness. In the vicinity of the Helmholtz resonance frequency, the duct is much shorter than the wavelength of sound; thus, the gas moves uniformly in the duct along its length and the moving mass is  $m = \rho A_d L_d$ , where  $\rho$  is the density of the gas. The stiffness is the restoring force divided by the displacement of the inertial element. If the inertial element is displaced by  $\Delta x$  from chamber  $V_1$  towards chamber  $V_2$ , a volume of gas  $A_d \Delta x$  is removed from chamber  $V_1$  and injected into chamber  $V_2$ . This produces a pressure difference between the chambers given by

$$\Delta p = \frac{A_d \Delta x}{k_s} \left( \frac{1}{V_1} + \frac{1}{V_2} \right), \quad (4)$$

where  $k_s \equiv -(\partial V/\partial p)_s/V$  is the adiabatic compressibility of the gas. The corresponding stiffness is  $\Delta p A_d/\Delta x$ ; thus, the frequency of the oscillation is given by

$$\omega_0^2 = \frac{\text{stiffness}}{\text{mass}} = \frac{A_d}{k_s \rho L_d} \left( \frac{1}{V_1} + \frac{1}{V_2} \right). \quad (5)$$

Equation (5) leads to Eq. (1) upon substitution of  $c_0^2$  for  $1/(k_s \cdot \rho)$ .

To estimate the viscous energy loss in the duct, we assume, for simplicity, that the duct is a circular cylinder with radius  $r_d$ . In the limit that  $\delta_v \ll r_d$ , the velocity of most of the gas is uniform across the duct. However, in the boundary layer in contact with the wall of the duct, the acoustic velocity  $v$  decays exponentially to zero with the characteristic length  $\delta_v$ . For the case of a plane surface with a tangential acoustic velocity  $v$  far from the surface, the viscous dissipation rate<sup>5</sup> per unit area is  $\frac{1}{2}(\eta/\delta_v)v^2$ . Using this result as an approximation for the cylindrical duct, the ratio of the viscous energy loss per cycle to the stored energy is

$$\alpha_v = \frac{\frac{1}{2}(\eta/\delta_v)v^2 \cdot 2\pi r_d L_d (2\pi/\omega)}{\frac{1}{2}\rho v^2 \pi r_d^2 L_d} = 2\pi \frac{\delta_v}{r_d}. \quad (6)$$

The ratio  $\alpha_v \equiv 2\pi/Q_v$  is the most significant contribution to reducing the quality factor  $Q$  of the Helmholtz oscillations.

To estimate the energy dissipated in the thermal boundary layer, we note that the temperature oscillates in phase with the pressure oscillation in each chamber of the Greenspan viscometer. However, in the thermal boundary layer in contact with the metal walls of the chambers, the temperature oscillations decay exponentially to zero with the characteristic length  $\delta_t$ . The ratio of the energy dissipated in the thermal boundary layer to the energy stored by creating a pressure difference between the chambers  $\alpha_t \equiv 2\pi/Q_t$  is the second most important contribution to reducing the  $Q$  of the Helmholtz oscillations. The heat transported from the gas to the boundary of a chamber during half of an acoustic cycle is approximately the product: (acoustic temperature change)  $\times$  (heat capacity/volume)  $\times$  (volume of the thermal boundary layer of the chamber). These terms are approximated by  $(\gamma-1)p_a k_s/\beta$ ,  $\rho C_p$ , and  $\delta_t A_{\text{ch}}$ , respectively. Here,  $\gamma \equiv C_p/C_v$  is the heat capacity ratio,  $p_a$  is the amplitude of the acoustic pressure,  $A_{\text{ch}}$  is the surface area of a chamber, and  $\beta \equiv (\partial V/\partial T)_p/V$  is the volume expansivity, respectively. Of this heat transported, a fraction on the order of (acoustic temperature change)/(temperature) is dissipated in the boundary layer. The potential energy stored is  $\frac{1}{2}p_a^2 V_{\text{ch}} k_s$  where  $V_{\text{ch}}$  is the volume of one chamber. These estimates are combined to obtain

thermal dissipation  
potential energy

$$= \frac{[(\gamma-1)k_s p_a/\beta] \rho C_p \delta_t A_{\text{ch}} (\gamma-1)k_s p_a/\beta}{\frac{1}{2}p_a^2 V_{\text{ch}} k_s T}, \quad (7)$$

and finally,

$$\alpha_t = 2 \frac{(\gamma-1)\delta_t A_{\text{ch}}}{V_{\text{ch}}}. \quad (8)$$

In arriving at Eq. (8), we have used the thermodynamic relation  $\rho C_p = T\beta^2/[k_s(\gamma-1)]$ .

The viscous and thermal losses may be combined to estimate the  $Q$  of the Helmholtz resonance. We obtain the simple result:

$$\frac{2g}{f_0} = \frac{1}{Q} = \frac{\alpha_v}{2\pi} + \frac{\alpha_t}{2\pi} = \frac{\delta_v}{r_d} + (\gamma-1) \frac{\delta_t A_{\text{ch}}}{\pi V_{\text{ch}}}. \quad (9)$$

The chambers of all of the viscometers were cylinders with lengths not very different from their diameters; thus, we estimate  $A_{\text{ch}}/V_{\text{ch}} = 3/r_{\text{ch}}$ , where  $r_{\text{ch}}$  is the radius of the chamber. Equation (9) implies that the Greenspan viscometer is indeed a viscometer, because the viscous contribution to the losses is much greater than the thermal contribution to the losses. For dilute gases,  $\delta_v$  and  $\delta_t$  have similar magnitudes and  $(\gamma-1)$  is at most  $\frac{2}{3}$ , its value for dilute monatomic gases. (Near the critical point,  $\gamma$  becomes very large.) Under the conditions of the present measurements with propane,  $(\gamma-1) \approx 0.1$  and  $r_d/r_{\text{ch}} \approx 0.05$ . Thus, the ratio of the thermal term in Eq. (9) to the viscous term in Eq. (9) is approximately 0.005.

A useful design equation is obtained by combining Eq. (2) for  $\delta_v$  and the viscous term in Eq. (9):

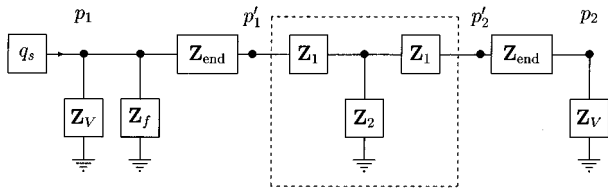


FIG. 4. Equivalent circuit of the Greenspan viscometer. The duct is represented by the “ $T$ ” equivalent circuit for a transmission line shown within the dashed box. The  $T$  parameters  $Z_1$  and  $Z_2$  are defined in the text. The source  $q_s$  drives the three parallel impedances: (1) the cavity impedance  $Z_v$ , (2) the duct represented as an end impedance  $Z_{\text{end}}$  in series with the  $T$  equivalent circuit, and (3) a parallel duct  $Z_f$  representing the fill capillary.

$$D_v = \eta/\rho = \pi f_0 (r_d/Q_v)^2. \quad (10)$$

Equation (10) shows that  $D_v$  may be determined by combining a measurement of  $r_d$  with frequency-response data from which  $f_0(1/Q)^2$  is obtained.

Even in the limit  $\delta_v \ll r_d$ , additions to the heuristic argument are required for accurate work. The viscous and thermal losses shift the resonance frequency from the result in Eq. (5); however, Eq. (9) is still correct to first order in  $\delta_v/r_d$  and  $\delta_t/r_{\text{ch}}$ . The converging and diverging flow in the transition regions where the duct joins the cavities increases the mass of the oscillating gas by a factor of approximately  $(1 + 1.598 r_d/L_d)$ . (In this work,  $0.02 \leq r_d/L_d \leq 0.04$ .) The coefficient 1.598 was determined through numerical calculations.<sup>6</sup> It depends weakly on the dimensions of the cavity and the duct, effects that were treated correctly in the analysis but neglected in the present discussion. Furthermore, there is excess viscous dissipation in the transition region, both inside the duct orifice and in the chamber near the orifice. The excess dissipation increases  $\alpha_v$  by a factor of approximately  $(1 + 1.6 r_d/L_d)$ . Finally, one must also account for the duct that is used to admit gas to the viscometer.

### III. OUTLINE OF DETAILED MODEL

In a more detailed calculation to be presented elsewhere,<sup>7</sup> we assumed that the acoustic source strength  $q_s$  generated by the transducer in chamber  $V_1$  is proportional to the voltage driving the source transducer. We also assumed that the complex voltage generated by the detector transducer is proportional to the pressure  $p_2$  at the detector located in chamber  $V_2$ . A calculation showed that the pressure at the inlet of the duct is very well approximated by the average pressure in  $V_1$  and that the pressure at the detector is similarly well approximated by the pressure at the outlet of the duct.

Our model of the Greenspan viscometer is the network of acoustic impedances shown schematically in Fig. 4. The ratio  $p_2/q_s$  is computed from this model. Here, we identify the elements in the network and the functional forms of their impedances.

The input impedance of each chamber  $Z_v$  is

$$Z_v = \rho c^2 / i\omega V, \quad (11)$$

with

$$V = V_{\text{ch}} + (1-i)(\gamma-1)A_{\text{ch}}\delta_t/2. \quad (12)$$

The complex volume  $V$  differs from the geometrical volume by a term that accounts for the admittance of the thermal boundary layer on the surfaces of the chamber.

The impedances of ducts are modeled as transmission lines with a characteristic impedance  $Z_0$  and a complex propagation parameter  $\Gamma$  for acoustic flow in the duct given by

$$Z_0 = (\rho c/A_d) / \sqrt{(1-F_v) \cdot [1 + (\gamma-1)F_t]},$$

$$\Gamma = \frac{i\omega}{c} \sqrt{\frac{1 + (\gamma-1)F_t}{1-F_v}}, \quad (13)$$

$$F = \frac{2J_1(\zeta)}{\zeta J_0(\zeta)},$$

where  $J_0$  and  $J_1$  are Bessel functions and  $\zeta \equiv (1-i)\delta_v/r_d$  for  $F_v$  and  $\zeta \equiv (1-i)\delta_t/r_d$  for  $F_t$ . The approximations

$$F_v \approx (1-i)\delta_v/r_d, \quad F_t \approx (1-i)\delta_t/r_d \quad (14)$$

are useful for the comparatively small values of  $\delta_v/r_d$  and  $\delta_t/r_d$  encountered in this work.

The  $T$  parameters (Fig. 4) for the duct are given by

$$Z_1 = Z_0 \tanh(\Gamma L_d/2), \quad Z_2 = Z_0 / \sinh(\Gamma L_d). \quad (15)$$

The inertial and dissipative end effects are described by

$$Z_{\text{end}} = (\rho\omega/A_d)(i\delta_i + 0.81\delta_v), \quad (16)$$

where  $\delta_i$  is defined by Eq. (17) below and, in this work,  $\delta_i \approx 0.8r_d$ .

The dissipative part of  $Z_{\text{end}}$  was computed from numerical solutions of the Helmholtz equation with Neumann boundary conditions and the geometry of the viscometers. The solutions provided a dissipation-free model for the acoustic pressure. The losses were determined by integrating the square of the tangential acoustic velocity. The coefficient 0.81 of  $\delta_v$  in Eq. (16) is the sum of two terms: the first, 0.45, is the contribution of the tangential flow on the chamber wall (“baffle”); the second, 0.36, is the contribution from the evanescent waves just inside the orifice.

There is an integrable singularity in the velocity at the sharp corner where the duct joins the chamber. If the corner is rounded with a radius equal to  $0.1r_d$ , the coefficient 0.81 in Eq. (16) is reduced to 0.74. This change is significant; it implies that chamfers often used in machine shop practice must be accounted for.

The reactive part of  $Z_{\text{end}}$  can be calculated from the numerical determinations of either the eigenvalue or the input impedance of the cavity. As noted above, the reactive term depends weakly on cavity dimensions. The results of the numerical calculations are accurately described by the function

$$\frac{\delta_i}{r_d} = 0.8215 - 1.107 \frac{r_d}{r_{\text{ch}}} + \frac{L_{\text{ch}} r_d}{3r_{\text{ch}}^2}. \quad (17)$$

The constant term in this expression agrees with the literature value obtained through solutions of the Laplace equation for a duct coupled to an infinite baffle.<sup>8</sup> The second term shows the effect of a chamber radius, in good agreement with the calculation of Ingard.<sup>9</sup> The third term comes from a

TABLE I. Dimensions of the viscometer in mm.

| Viscometer | $L_d$  | $r_d$  | $L_{ch}$ | $r_{ch}$ |
|------------|--------|--------|----------|----------|
| 0          | 38.092 | 0.7998 | 31.565   | 15.873   |
| 1          | 19.109 | 0.7976 | 15.749   | 15.875   |
| 2          | 28.586 | 0.7985 | 15.769   | 15.876   |
| 5          | 28.531 | 0.8267 | 31.582   | 15.876   |

correction to the chamber's input impedance due to the finite length of the chamber. The sum of the three terms varies between 0.782 and 0.799 for the four viscometers used in the current work.

As shown in Fig. 4, the fill duct can be represented by an impedance  $Z_f$  in parallel with  $Z_v$ . To do this, the fill duct can be replaced with a second  $T$  equivalent network with propagation parameters appropriate for its very small radius. In this case, the exact functional forms for  $F_f$  and  $F_v$  must be used. The complicated expression that results will not be reproduced here. The expression was included in the "working equation" used to analyze our data; however, the present results are not sensitive to the effects of our very long, thin fill duct.

A "working equation" was constructed that expresses the measured frequency-dependent voltage ratio,  $V_{\text{detector}}/V_{\text{source}}$ , as the product:

$$\frac{V_{\text{detector}}}{V_{\text{source}}} = \frac{V_{\text{detector}}}{p_2} \times \frac{p_2'}{p_2'} \times \frac{p_1'}{p_1'} \times \frac{p_1}{V_{\text{source}}}. \quad (18)$$

The acoustic pressure ratios in Eq. (18) were expressed as functions of the impedances defined above for the network in Fig. 4. The two ratios,  $V_{\text{detectors}}/p_2$  and  $p_1/V_{\text{source}}$ , that characterize the transducers were shown to be independent of frequency by auxiliary measurements using an acoustic coupler.

## IV. APPARATUS AND MEASUREMENTS

### A. Construction of viscometers

Figure 1 shows a cross section of viscometer 1. The body of the viscometer was turned on a lathe from a single piece of aluminum. The duct was drilled undersized and then reamed to its final size. The interior surfaces of the viscometer were not polished.

The dimensions of the viscometers' bodies were measured with a coordinate measuring machine. The machine logged the coordinates of surfaces that were contacted by a 1.4-mm-diam ruby ball. The internal diameters of the ducts were measured at 1 mm intervals along the axes of the ducts.

Table I summarizes the key dimensions of the viscometers. Except for their dimensions, all four viscometers were essentially identical.

### B. Transducers

Two brass flanges containing transducers were used as interchangeable ends of all of the viscometers. These flanges were bolted to the body of the viscometer using blind tapped holes that are not shown in Fig. 1. The joints between the flanges and the body were sealed with a thin layer of organic

grease. Efforts were made to avoid scratches and crevices that might attenuate the acoustic oscillations. (Scratches, pits, etc. with at least one dimension smaller than  $\delta_v$  are probably not important to the operation of Greenspan viscometers.)

Both transducers were installed in ports machined out of each flange. The acoustic source was a "stack" of coin-shaped piezoelectric transducers (PZT) connected mechanically in series and electrically in parallel. The length of the stack changed in response to the applied voltage. The stack was separated from the test gas in chamber  $V_1$  by a 0.1-mm-(0.004-in.)-thick  $\times$  15-mm-diam stainless-steel foil that had been soldered into a slight recess in the interior face of the flange. The acoustic detector was a thin cylindrical bimorph PZT that had been removed from a commercial buzzer. The detector was sealed behind a foil that faced the inside surface of  $V_2$ . Thus, the test gas within the viscometers was in contact with robust metal parts only: the viscometer body, the flanges, and the foils.

Under typical operating conditions (viscometer 1, argon, 100 kPa), the source was driven at 46 V (rms), and it generated an acoustic pressure on the order of 0.4 Pa (rms). Allowing for the  $Q$  of the double Helmholtz resonator and the volume of chamber  $V_1$ , we estimated that the volume displaced by the source transducer was 0.014 mm<sup>3</sup>.

Under a variety of conditions, we reduce the drive voltage by a factor of 10 and repeated the measurements of the frequency response. No changes were detected, confirming that during normal operation, the Greenspan viscometer can be described by linear acoustics despite the presence of fairly sharp corners at the ends of the duct.

In common with other studies of acoustic resonators,<sup>10</sup> the signal-to-noise ratio varied as  $P^{3/2}$ . To understand this, we note that, to a good approximation, the displacement produced by the source transducer was independent of  $P$ . Thus, well below  $f_0$ , the acoustic pressure  $p_a$  in chamber  $V_1$  was proportional to  $P$ . Near resonance, where the viscometer was used,  $p_a$  was amplified by a factor of  $Q$ , which itself was proportional to  $P^{1/2}$ . Even at the lowest pressures studied, the signal-to-noise ratio was not a factor limiting the accuracy of the determination of the viscosity.

### C. Test conditions

To test several viscometers with several gases, we constructed a pressure vessel with an interior volume of approximately 1800 cm<sup>3</sup>. The viscometer under test was suspended inside the pressure vessel. This isolated the viscometer from ambient acoustic noise and relieved us of the necessity of making every viscometer pressure tight.

The temperature of the viscometer under test was determined by a calibrated thermistor that had been inserted into a blind hole drilled into the viscometer's body. When the viscometer was suspended in the pressure vessel, the thermal relaxation time between the viscometer and the ambient air was 5 h. In effect, the viscometer was thermally isolated from the room on the time scale of the viscosity measurements.

For a typical test run, the pressure vessel was filled with the test gas at the highest pressure to be studied (1 MPa for

helium and argon; 600 kPa for propane), 15 min were allowed to elapse for thermal equilibration, and then the frequency response, temperature, and pressure were measured. Then, some of the test gas in the pressure vessel was removed and the operations were repeated. As the measurements progressed, the temperature of the viscometer decreased several tenths of a degree because of the adiabatic cooling of the test gas as the pressure was reduced. The thermometer in the body of the viscometer enabled us to measure this effect.

#### D. Fill capillary

A fill capillary led from chamber  $V_1$  to the interior of the pressure vessel. If the flow impedance of the capillary had not been sufficiently great near the Helmholtz resonance frequency, the capillary would have functioned as a second duct in parallel with the duct between the two chambers. The second duct would have greatly altered the frequency response of the viscometer and a second Helmholtz resonance might have appeared. To achieve a high impedance, we used a stainless-steel capillary with an o.d. of 0.029 in. (0.74 mm), an i.d. of 0.016 in. (0.41 mm), and a length of 10 cm. The capillary was sealed into a hole that had been drilled through the body of the viscometer.

#### E. Frequency response measurements

For each viscometer, gas, and thermodynamic state, the complex frequency response of the viscometer was measured at 21 equally spaced frequencies that spanned the range  $f_m \pm 2g$ , where  $f_m$  was the frequency at which the detected signal attained its maximum amplitude. These measurements were made with a computer-controlled frequency synthesizer, lock-in amplifier, and digital voltmeter, using techniques that we have described elsewhere.<sup>11</sup> Because the step-up transformer connected between the frequency synthesizer and the source transducer did not have a flat frequency response at low frequencies, one change was required. The detector output voltage was divided by the voltage measured at the source transducer at each frequency.

The real and imaginary parts of the measured frequency response, such as that displayed in Fig. 3, were simultaneously fit by Eq. (18) with the addition of a complex background term that was either a constant or a linear function of frequency. (A constant background term was adequate for all the data except the helium data taken with viscometer 0.) Thus, either 6 or 8 parameters were fitted to the data. Two parameters characterize the frequency and width of the Helmholtz resonance; two comprise a complex amplitude that accounts for the gain of the electronics and transducers; and the two or four background parameters account for electrical and mechanical crosstalk between the transducers.

Figure 3 displays a typical example of the measured frequency response of viscometer 1 together with the deviations of the data from our model. The model represents the data with very small systematic fractional deviations on the order of  $\pm 0.0005$ . The fit defines values of  $g$  and  $f_m$  with fractional imprecisions of 0.0005 and  $0.0005 \times g/f_m \approx 3.5 \times 10^{-5}$ , respectively. The imprecision of 0.0005 in  $g$

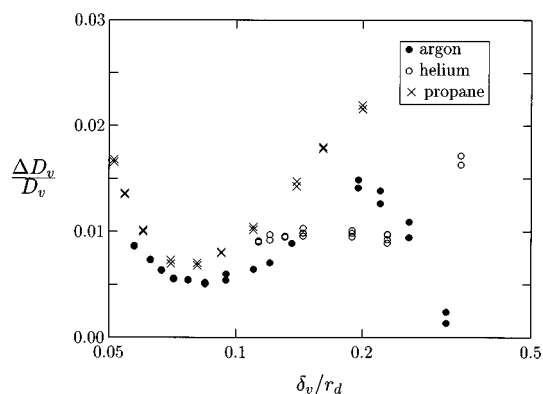


FIG. 5. Values of  $D_v \equiv \eta/\rho$  measured with viscometer 1 minus the values from the literature for three gases as a function of  $\delta_v/r_d$ , the ratio (viscous penetration length)/(radius of duct). The data for the three gases cluster about  $\delta D_v/D_v = 0.01$ , except for the data at the lowest pressures ( $\delta_v/r_d > 0.22$ ), where the  $Q$ 's of the resonances are smallest.

corresponds to an imprecision of 0.001 in  $D_v$ ; the imprecision of  $3.5 \times 10^{-5}$  in  $f_m$  corresponds to an imprecision of  $3.5 \times 10^{-5}$  in the speed of sound  $c_0$ . At the present time, imperfections in the model for the viscometer make the results more uncertain than these very small values.

#### V. RESULTS

Figure 5 displays the results for  $D_v$  obtained with viscometer 1, the “best” viscometer. In each case, the plot shows the fractional deviations of the measured values of  $D_v$  from values taken from the literature. Nearly all the results for helium, argon, and propane fall within a band  $\pm 0.005$  wide centered 0.010 above the data from the literature. The ordinate for Fig. 5 is  $\delta_v/r_d \approx 1/Q$ , which is the most important parameter determining the frequency response function. Remarkably, for the smallest values of  $\delta_v/r_d$  that occur at the highest pressures, the data for argon and the data for propane track within 0.3%. At the larger values of  $\delta_v/r_d$ , the data for the different gases diverge. The larger values of  $\delta_v/r_d$  occur at low pressures where the viscous boundary layer fills the duct nearly completely. Under these conditions, the  $Q$ 's of the resonances are low and the need to properly account for the frequency responses of the transducers becomes severe. Thus, we do not recommend using Greenspan viscometers at larger values of  $\delta_v/r_d$ .

Figure 6 displays the results for  $D_v$  obtained with viscometer 0, the “worst” viscometer. Again, nearly all the results for helium, argon, and propane fall within a band  $\pm 0.005$  wide; however, for this viscometer, the data are centered approximately 0.025 above the data from the literature.

At present, we have no certain explanation for why the data from the viscometers differ from each other. The data for the other viscometers that we have studied fall between the data for viscometer 1 and viscometer 0. In the future, we shall report the results of systematic investigations of the effects of surface finish and of the “end corrections” for the converging/diverging flow fields near the ends of the duct. The ducts of all of our viscometers had crude chamfers at their ends that were not considered when analyzing the data.

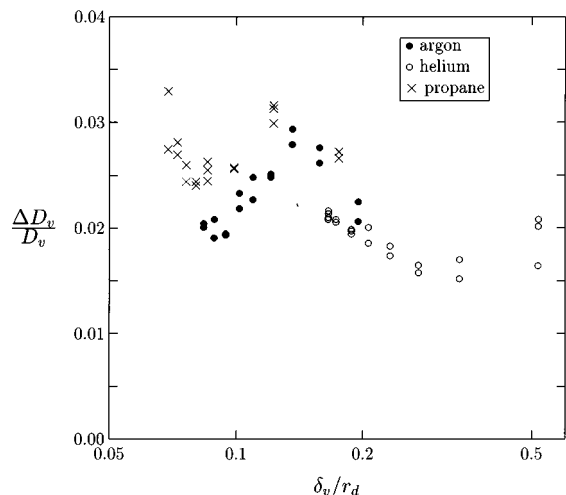


FIG. 6. Values of  $D_v \equiv \eta/\rho$  measured with viscometer 0 minus the values from the literature for three gases as a function of  $\delta_v/r_d$ , the ratio (viscous penetration length)/(radius of duct). The data for the three gases cluster about  $\Delta D_v/D_v = 0.025$ .

In order to construct Figs. 5 and 6, we used information from the literature for  $D_v$ . For argon, the zero-density viscosity was calculated for the HFD-B3 potential of Aziz and Slaman,<sup>12</sup> and the density dependence was taken from Maitland *et al.*<sup>13</sup> For helium, the zero-density viscosity was calculated from the potential of Ref. 2 and the density dependence was taken from Ref. 13. For propane, the correlation by Vogel<sup>14</sup> was used. Because Vogel calibrated his viscometer with the data of Kestin *et al.*,<sup>15</sup> his correlation (at low pressures) agrees within  $\pm 0.1\%$  with the data of Kestin *et al.* Thus, the literature values of the viscosity for the three different gases are ultimately traceable to the same laboratory and their mutual consistency is likely to be greater than their absolute accuracy. As mentioned above and in Ref. 2, the viscosity data for helium near ambient temperature appear to have a systematic error of only 0.3%.

If each viscometer had been calibrated with a single gas at a single temperature and at a pressure with a comparatively small value of  $\delta_v/r_d$ , then nearly all the results for  $D_v$  from that viscometer for all three gases would have been within  $\pm 0.5\%$  of the data from the literature.

Figure 7 shows the deviations of the fitting parameter  $f_0$  for the frequency response data from viscometers 0 and 1 from the values predicted from the measured dimensions of the viscometers, the speed of sound in the test gases, and the model given by Eq. (18). The fractional deviations of  $f_0$  from their expected values and the small inconsistencies of the results among the three gases are very approximately the same size as the deviations of the values of  $D_v$ ; the deviations may have the same, presently unknown, cause.

## VI. PROSPECTS FOR A PRIMARY STANDARD GREENSPAN VISCOMETER

As just mentioned, the results from the “best” viscometer contain several puzzles that we hope will be resolved by further research. If they are, the performance of the Greenspan viscometer will approach those of other standard

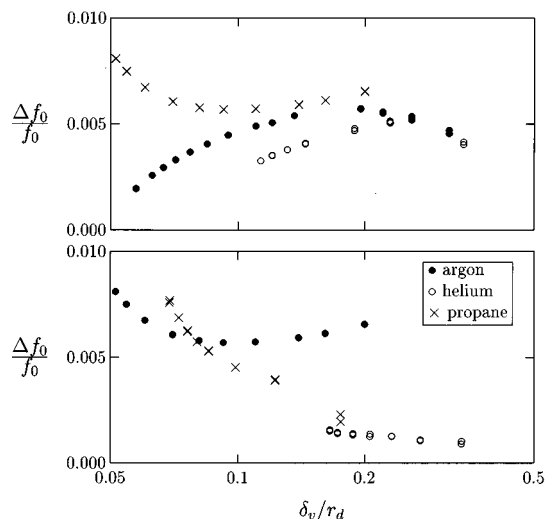


FIG. 7. Deviations of the fitted resonance frequencies  $f_0$  from those calculated from Eq. (18). Top: results from viscometer 0; bottom: results from viscometer 1.

viscometers. In this spirit, we contrast the Greenspan viscometer with current standards and consider directions for further development.

The presently accepted instrument for making absolute measurements of the viscosity of gases is based upon a disk that oscillates between fixed plates while suspended from a delicate quartz fiber.<sup>16</sup> This instrument has a thoroughly developed theory that accounts for the “edge corrections” resulting from the finite dimensions of the disk. The geometry of the oscillating-disk viscometer is designed to inhibit secondary flow resulting from either the very low frequency ( $\sim 0.1$  Hz) oscillations or from temperature gradients. However, oscillating-disk viscometers are difficult to maintain. To the authors’ knowledge, there is no longer a primary standard oscillating disk viscometer in operation. The oscillating disk viscometers are ordinarily excited with an impulse and the subsequent free decay of the oscillations is observed. In contrast with the present study of the Greenspan viscometer, we are not aware of studies of the frequency response of the oscillating disk viscometer directed towards testing the theory of its operation.

As indicated above, the Greenspan viscometer is rugged and prototypes are easily constructed. The theory for the Greenspan viscometer contains corrections for the acoustic flows near the ends of the ducts that are comparable in magnitude to the edge corrections needed for the oscillating-disk viscometer. A comparatively simple modification of the present Greenspan viscometer will facilitate systematic studies of the effects of the flows at the ends of the duct. Such a modification is shown in Fig. 8, top.

Figure 8, top, shows a schematic drawing of a Greenspan viscometer with a removable duct. We are constructing such an instrument as a convenient platform for systematically testing the theory of “end” corrections that scale with  $r_d/L_d$ . Furthermore, the approach shown in Fig. 8 (top) is suitable for using very sophisticated cylinders as ducts. For example, precision cylinders manufactured for use

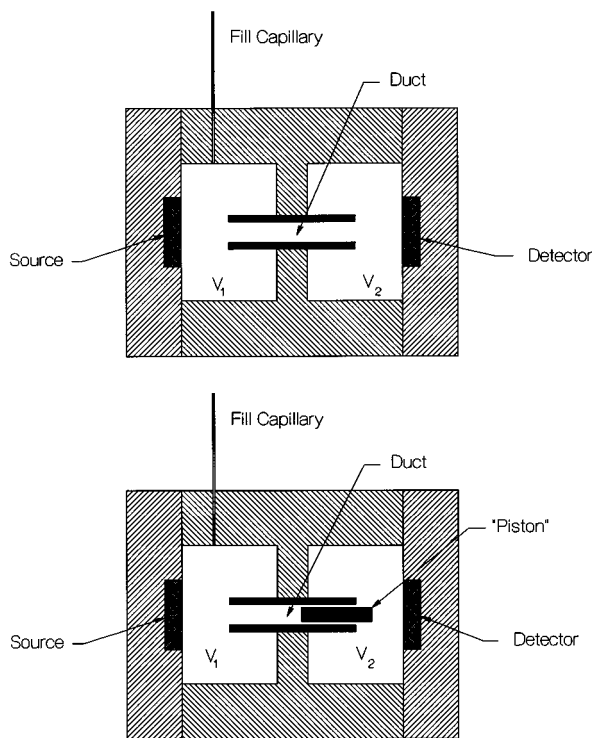


FIG. 8. Top: cross section of Greenspan viscometer with removeable duct. An accurately characterized cylinder such as those used in dead-weight pressure gauges could be used as the duct. Bottom: cross section of Greenspan viscometer with a moveable rod partially inserted into the duct.

in dead-weight pressure gauges are lapped until their surfaces have scratches that are 50 nm or even finer. The deviations from roundness and internal diameters of such high-quality cylinders can be determined to several parts in  $10^5$ . Such a cylinder could be used as the duct of a Greenspan viscometer. (The duct of an acoustic viscometer may have a diameter that is much larger than that of the capillary tube used in unidirectional flow viscometers. This design flexibility exists because the viscous dissipation in the acoustic viscometer occurs within a thin boundary layer of thickness  $\delta_t$  surrounding the perimeter of the duct. In contrast, the dissipation in a unidirectional flow viscometer occurs throughout the capillary.)

Finally, we mention a way in which the concept of differential metrology can be applied to the Greenspan viscometer. One can construct a Greenspan viscometer in which a solid rod, i.e., a piston, partially fills a duct. Figure 8, bottom, shows the design of such a viscometer. In this design, the

gap between the rod and the duct is significantly larger than  $\delta_v$  everywhere, and the rod can be supported in two or more configurations such that one end is within the duct and the other end is within one of the chambers. One would measure the frequency response of such a Greenspan viscometer when the rod occupies several different known positions along the axis of the cylinder. The converging/diverging flow fields near the ends of the duct and near the ends of the rod are unchanged upon displacing the rod axially; thus, the effects of these difficult-to-model portions of the flow field will cancel out of the difference measurements to a high degree. The differences could be more accurately related to the viscosity than any single measurement.

## ACKNOWLEDGMENTS

This research was supported in part by the Office of Naval Research. The authors thank Dr. T. Doiron and E. Erber of NIST's Manufacturing Engineering Laboratory for using a coordinate measuring machine to determine the dimensions of the prototype viscometers. We also thank Stephen Boyes for his help with data acquisition during the early stages of this work.

- <sup>1</sup>M. Greenspan and F. N. Wimenitz, "An Acoustic Viscometer for Gases-I," NBS Report 2658 (1953).
- <sup>2</sup>R. A. Aziz, A. R. Janzen, and M. R. Moldover, *Phys. Rev. Lett.* **74**, 1586 (1995).
- <sup>3</sup>W. A. Wakeham, A. Nagashima, and J. V. Sengers, *Measurements of the Transport Properties of Fluids* (Blackwell Scientific, Oxford, 1991), Chap. 3.
- <sup>4</sup>K. A. Gillis, M. R. Moldover, and A. R. H. Goodwin, *Rev. Sci. Instrum.* **62**, 2213 (1991).
- <sup>5</sup>P. M. Morse and K. U. Ingard, *Theoretical Acoustics* (McGraw-Hill, New York, 1968), Sec. 6.4.
- <sup>6</sup>J. B. Mehl, *J. Acoust. Soc. Am.* **97**, 3327 (1995) and unpublished calculations.
- <sup>7</sup>J. B. Mehl, K. A. Gillis, and M. R. Moldover (to be published).
- <sup>8</sup>L. V. King, *Philos. Mag. Ser. 7* **21**, 128 (1936).
- <sup>9</sup>U. Ingard, *J. Acoust. Soc. Am.* **25**, 1037 (1953).
- <sup>10</sup>M. R. Moldover, J. P. M. Trusler, T. J. Edwards, J. B. Mehl, and R. S. Davis, *J. Res. Natl. Bur. Stand.* **93**, 85 (1988).
- <sup>11</sup>M. R. Moldover, J. B. Mehl, and M. Greenspan, *J. Acoust. Soc. Am.* **79**, 253 (1986).
- <sup>12</sup>R. A. Aziz and M. J. Slaman, *J. Chem. Phys.* **92**, 1030 (1990).
- <sup>13</sup>G. C. Maitland, R. Rigby, E. B. Smith, and W. A. Wakeham, *Intermolecular Forces: Their Origin and Determination* (Clarendon, Oxford, 1981), Appendix 4, Table A4.3.
- <sup>14</sup>E. Vogel, "The Viscosity of Gaseous Propane and its Initial Density Dependence," Proceedings of the 12th Symposium on Thermophysical Properties, Boulder, Colorado, June 19–24, 1994.
- <sup>15</sup>J. Kestin, S. T. Ro, and W. A. Wakeham, *Trans. Faraday Soc.* **67**, 2308 (1971).
- <sup>16</sup>Reference 3, pp. 25–31.